

---

# TI-DeepONet: Learnable Time Integration for Stable Long-Term Extrapolation

---

**Dibyajyoti Nayak**

Department of Civil and Systems Engineering  
Johns Hopkins University  
Baltimore, MD, 21218  
dnayak2@jh.edu

**Somdatta Goswami**

Department of Civil and Systems Engineering  
Johns Hopkins University  
Baltimore, MD, 21218  
sgoswam4@jhu.edu

## Abstract

Accurate temporal extrapolation presents a fundamental challenge for neural operators in modeling dynamical systems, where reliable predictions must extend significantly beyond the training time horizon. Conventional deep operator network (DeepONet) approaches employ two inherently limited training paradigms: fixed-horizon rollouts that predict complete spatiotemporal solutions while disregarding temporal causality, and autoregressive formulations that accumulate errors through sequential predictions. We introduce TI-DeepONet, a framework that integrates neural operators with adaptive numerical time-stepping techniques to preserve the Markovian structure of dynamical systems while substantially mitigating error propagation in extended temporal forecasting. Our approach reformulates the learning objective from direct state prediction to the approximation of instantaneous time-derivative fields, which are subsequently integrated using established numerical schemes. This architecture inherently supports continuous-time prediction and enables the deployment of higher-precision integrators during inference than those utilized during the training phase, balancing computational efficiency with predictive accuracy. We further develop TI(L)-DeepONet, which incorporates learnable coefficients for intermediate slopes in the numerical integration process, thereby adapting to solution-specific variations and enhancing predictive fidelity. Extensive evaluation across three canonical partial differential equations demonstrates that TI(L)-DeepONet marginally outperforms TI-DeepONet, with both methodologies significantly reducing relative  $L_2$  extrapolation errors, approximately 81% compared to autoregressive implementations and 70% compared to fixed-horizon approaches. Notably, both frameworks maintain prediction stability for temporal domains extending to roughly twice the training interval. This research establishes a physics-aware operator learning paradigm that effectively bridges neural approximation with numerical analysis principles while preserving the causal structure of dynamical systems, addressing a critical capability gap in the long-term forecasting of complex physical phenomena.

## 1 Introduction

Time-dependent partial differential equations (PDEs) are typically solved using spatial discretization (e.g., finite elements or volumes) combined with time-stepping schemes such as Runge–Kutta or Adams–Bashforth. While accurate, such solvers can be prohibitively expensive for high-dimensional or many-query problems. Explicit integrators are constrained by stability conditions (e.g., CFL), while implicit schemes require solving large systems of equations at each step. Moreover, classical solvers generalize poorly: each new initial or boundary condition requires a fresh simulation.

Neural operators (NOs) offer an attractive alternative by learning mappings from input functions (e.g., initial conditions) to solutions, bypassing discretization and enabling fast inference. Models like DeepONet [1] and FNO [2] have shown promise in parametric PDE settings. However, extending NOs to time-evolving systems introduces new challenges. The standard approach is to train a model that maps the solution at time  $t$  to the solution at time  $t + \Delta t$ , and roll this forward autoregressively (see Figure 1). Unfortunately, this approach suffers from severe error accumulation, as each prediction feeds into the next, compounding inaccuracies and often leading to instability. Alternatively, one can train a model to predict an entire trajectory (“full rollout”), which avoids stepwise feedback but tends to degrade in accuracy when extrapolating beyond the training time window. Crucially, most existing works [3, 2, 4, 1] only evaluate models within the training time span, neglecting the need for reliable extrapolation, a capability that is essential for real-time engineering applications and control tasks. Moreover, existing work [5, 6, 7] on autoregressive and full rollout operator models tends to impose a discrete-time Markovian assumption, which misaligns with the underlying continuous-time dynamics of PDEs. These limitations often result in unstable or inaccurate long-term predictions. Thus, a key barrier remains: NOs struggle not only with long-horizon accuracy but also with extrapolating into unseen temporal domains, a prerequisite for trustworthy deployment.

Several recent works attempt to address these limitations. For example, Diab et al. [8] augment DeepONet with an additional temporal branch to capture dependencies, while Michalowska et al. [9] employ recurrent networks (RNNs, LSTMs, GRUs) atop neural operator outputs to better handle sequences. Other approaches introduce memory modules [10, 11, 12] to compensate for the non-Markovian nature of rollout-based methods. However, these strategies largely rely on generic time-series architectures rather than tackling the issue from a dynamical systems perspective.

In this work, we introduce a novel approach inspired by classical numerical analysis. Our proposed TI-DeepONet framework embeds time integration directly into the operator learning process for dynamical systems. Rather than predicting future solution states directly, we train a DeepONet to approximate the instantaneous time derivative  $\partial u / \partial t$ . During training, this derivative operator is coupled with a Runge-Kutta numerical integrator to evolve the state forward in time. The predicted future state is then compared against the ground truth in the loss function, enabling the network to learn dynamics that respect temporal causality and numerical stability. At inference time, we leverage high-order multistep integrators (such as Adams-Basforth/Adams-Moulton predictor-corrector schemes) with refined timesteps to reliably propagate solutions based on the learned time derivative operator. This operator learning framework which maps between function spaces rather than from function spaces to vector spaces as in standard neural networks and neural ODEs [13] - provides the flexibility to modify time-stepping parameters between training and testing phases, thereby ensuring stable predictions. We further introduce TI(L)-DeepONet, an enhanced variant that incorporates learnable weighting coefficients conditioned on the system state at each timestep. This adaptation dynamically adjusts the integration process based on local solution characteristics.

While TI-DeepONet shares conceptual similarities with neural ODEs in learning time derivatives and using numerical integration, our approach differs significantly in both scope and implementation. Neural ODEs typically operate on low-dimensional latent states, whereas TI-DeepONet is specifically designed for high-dimensional spatiotemporal fields and learns an explicit operator mapping between function spaces. Furthermore, unlike neural ODEs, which treat the integrator as fixed, we explicitly embed the integrator within the solution operator, allowing us to employ different integration schemes at inference time according to accuracy and efficiency requirements.

We demonstrate the effectiveness of our approach on three benchmark PDEs – the 1D and 2D Burgers’ equations and the 1D Korteweg–de Vries (KdV) equation. Across all cases, TI-DeepONet and its adaptive variant TI(L)-DeepONet significantly outperform standard autoregressive and full rollout operator models, achieving stable long-term predictions and accurate extrapolation for time horizons approximately twice as long as the training interval.

## 2 Methodology

We consider a general time-dependent PDE governing the spatiotemporal evolution of a solution field. Let the solution  $u(\mathbf{x}, t)$  be defined over a temporal domain  $t \in [0, T]$  and spatial domain  $\mathbf{x} = [x_1, x_2, \dots, x_m] \in \mathcal{X} \subseteq \mathbb{R}^m$ . The dynamics of  $u$  are governed by a PDE that relates the

temporal derivative  $u_t$  to spatial derivatives  $u_{\mathbf{x}}, u_{\mathbf{xx}}, \dots$  via a general nonlinear function  $\mathcal{F}$ :

$$u_t = \mathcal{F}(t, \mathbf{x}, u, u_{\mathbf{x}}, u_{\mathbf{xx}}, \dots). \quad (1)$$

This work uses DeepONet to study error accumulation in autoregressive time-stepping. To mitigate this, we propose TI-DeepONet and TI(L)-DeepONet, which significantly reduce error growth and enable accurate long-term extrapolation. The following subsections introduce these architectures.

## 2.1 Deep Operator Network (DeepONet)

Deep Operator Network (DeepONet) are grounded in the universal approximation theorem for nonlinear operators [14], and are designed to learn mappings between infinite-dimensional input and output function spaces. A standard DeepONet architecture comprises two subnetworks: a branch network and a trunk network. The branch network encodes the input function  $\mathbf{v}(\eta)$ , evaluated at a set of fixed sensor locations  $\{\eta_1, \eta_2, \dots, \eta_m\}$ , producing a set of coefficient weights. The trunk network takes as input the query coordinates  $\zeta = (x, y, z, t)$  and outputs the corresponding basis functions.

The goal of DeepONet is to learn an operator  $\mathcal{G}(\mathbf{v})$  such that, for any input realization  $\mathbf{v}_j$ , the output is a scalar-valued function evaluated at arbitrary spatiotemporal locations  $\zeta$ . The predicted solution is computed as the weighted inner product of the outputs of the two networks defined as:  $\mathcal{G}_{\theta}(\mathbf{v}_j)(\zeta) = \sum_{i=1}^p br_i(\mathbf{v}_j(\eta_1), \dots, \mathbf{v}_j(\eta_m)) \cdot tr_i(\zeta)$ , where  $br_i(\cdot)$  and  $tr_i(\cdot)$  denote the outputs of the branch and trunk networks, respectively, and  $\theta$  represents all trainable parameters.

In general, operator learning frameworks like DeepONet aim to learn a solution operator that maps any functional input, such as initial conditions (ICs), boundary conditions (BCs), or source terms, to the corresponding spatiotemporal solution field. However, this mapping is inherently non-causal with respect to time: the operator does not explicitly enforce the Markovian nature of dynamical systems, where the future state depends on the present (or past) states. As a result, direct operator prediction over time often fails to preserve temporal coherence, particularly for long-term simulations.

To account for temporal dynamics, a common strategy is to use autoregressive prediction, where the model recursively predicts the next state using the current state as input. This approach aligns more closely with the natural evolution of dynamical systems and is illustrated schematically in Fig. 1. However, autoregressive rollouts are prone to error accumulation and often degrade over long horizons - a core motivation for our proposed time-integrated operator learning framework.

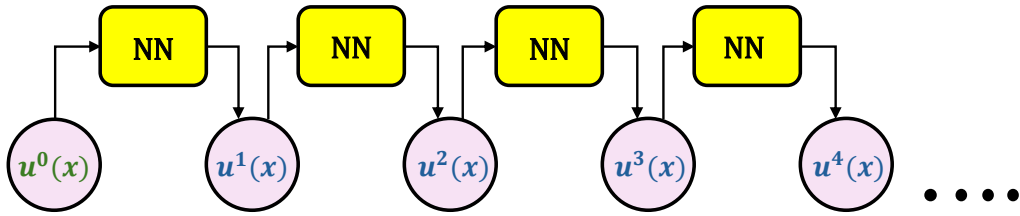


Figure 1: A schematic showing how autoregressive predictions in time are performed.

## 2.2 Time Integrator embedded Deep Operator Network (TI-DeepONet)

As discussed previously, full spatiotemporal rollouts from a single-step operator such as vanilla DeepONet are not physically meaningful, as they disregard the temporal dependencies between successive solution states. Additionally, autoregressive predictions suffer from error accumulation due to compounding approximation errors over time.

To mitigate these limitations, we propose the TI-DeepONet architecture. Rather than directly predicting the next state  $u^{i+1}$ , the network learns the right-hand side (RHS) of the time-dependent PDE (Eq. 1), i.e., the time derivative  $u_t = \mathcal{F}(t, \mathbf{x}, u, u_{\mathbf{x}}, u_{\mathbf{xx}}, \dots)$ . This learned derivative is passed to a numerical time integrator to compute the next solution state from the current one. In particular, we use the RK4 scheme to advance the solution in time. For a timestep  $\Delta t$ , the RK4 update rule is given by,  $k_1 = \mathcal{F}(t^i, u^i)$ ,  $k_2 = \mathcal{F}(t^i + \frac{\Delta t}{2}, u^i + \frac{\Delta t}{2}k_1)$ ,  $k_3 = \mathcal{F}(t^i + \frac{\Delta t}{2}, u^i + \frac{\Delta t}{2}k_2)$ ,  $k_4 = \mathcal{F}(t^i + \Delta t, u^i + \Delta t \cdot k_3)$ , and  $u^{i+1} = u^i + \Delta t (\frac{1}{6}k_1 + \frac{2}{6}k_2 + \frac{2}{6}k_3 + \frac{1}{6}k_4)$ . This formulation leads to an end-to-end differentiable pipeline, where the loss is computed between the predicted

solution  $\hat{u}^{i+1}$  and the ground truth  $u^{i+1}$ , and gradients are backpropagated through the time integrator to update the network parameters. However, the RK4 slope coefficients,  $\{\frac{1}{6}, \frac{2}{6}, \frac{2}{6}, \frac{1}{6}\}$ , are fixed.

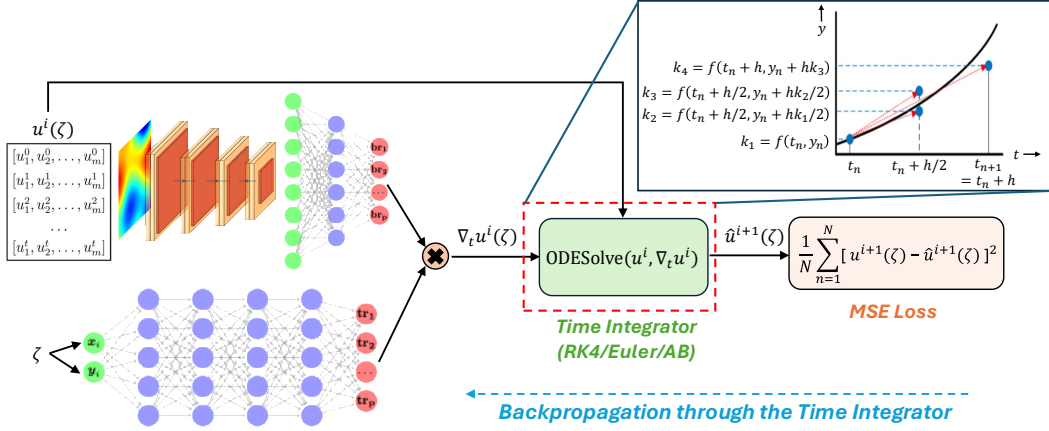


Figure 2: A schematic of the proposed TI-DeepONet architecture.

### 2.3 Learnable Time Integrator embedded Deep Operator Network (TI(L)-DeepONet)

To introduce flexibility into the integration process, we extend TI-DeepONet by making the Runge–Kutta weighting coefficients learnable and state-dependent. This leads to the development of TI(L)-DeepONet. Specifically, we replace the constant RK4 slope coefficients,  $\{\frac{1}{6}, \frac{2}{6}, \frac{2}{6}, \frac{1}{6}\}$ , with adaptive coefficients conditioned on the current solution state  $u^i$ . We introduce an auxiliary neural network,  $\text{MLP}_{\text{RK}}$ , which maps the current state to a set of four weights,  $\alpha = [\alpha_1, \alpha_2, \alpha_3, \alpha_4] = \text{MLP}_{\text{RK}}(u^i)$ . These weights are then used to compute the next solution state via:

$$u^{i+1} = u^i + \Delta t \cdot (\alpha_1 k_1 + \alpha_2 k_2 + \alpha_3 k_3 + \alpha_4 k_4). \quad (2)$$

For numerical stability and interpretability, we normalize the weights using softmax activation function, such that:  $\tilde{\alpha}_j = \frac{\exp(\alpha_j)}{\sum_{\ell=1}^4 \exp(\alpha_\ell)}$ ,  $\forall j = 1, 2, 3, 4$ . This adaptive scheme allows the model to adjust the influence of each intermediate slope dynamically, thereby compensating for the approximation error [15] of the DeepONet prediction, enabling more robust predictions in stiff, nonlinear, or highly transient regimes. For example, in regions with rapid spatial changes, the model may place greater weight on later-stage evaluations like  $k_4$ , while in smoother regions, earlier evaluations may suffice.

## 3 Results

To evaluate the efficacy of our framework, we consider three canonical PDEs: (1) 1D Burgers' equation, (2) 1D KdV equation, and (3) 2D Burgers' equation. Model performance is assessed using the relative  $L_2$  error, defined as  $\text{error} = \frac{\|u_{\text{pred}} - u_{\text{true}}\|_2}{\|u_{\text{true}}\|_2}$ , where  $u_{\text{pred}}$  and  $u_{\text{true}}$  denote the predicted and ground truth solutions, respectively. Table 1 and Figure 3 summarize the comparative training and extrapolation accuracy across all methods for all applications. To evaluate the statistical variability of the performance of the model, we report the mean and standard deviation of error metric in Table A2 based on five independent training trials. Additional details on data generation, training configurations, and network architecture are provided in Supplementary Information (SI) C. The code to reproduce the experiments is publicly available at <https://github.com/Centrum-IntelliPhysics/TI-DeepONet-for-Stable-Long-Term-Extrapolation.git>.

### 3.1 One-dimensional Burgers' Equation

The viscous Burgers' equation is a canonical PDE arising in fluid mechanics, nonlinear acoustics, and traffic flow. For the velocity field  $u(x, t)$  with viscosity  $\nu = 0.01$ , it is defined as:

$$\frac{\partial u}{\partial t} + u \frac{\partial u}{\partial x} = \nu \frac{\partial^2 u}{\partial x^2}, \quad (x, t) \in [0, 1] \times [0, 1], \quad (3)$$

Table 1: Relative  $L_2$  errors across frameworks in the extrapolation regime. TI-DeepONet AB employs RK4 during training and AB2/AM3 during inference.

Problem	$t_{train}^*$	$\Delta t_e^*$	Method	Relative $L_2$ error			
				$t+10\Delta t_e$	$t+20\Delta t_e$	$t+40\Delta t_e$	$T^*$
Burgers' (1D)	0.5	0.01	TI(L)-DeepONet [Ours]	<b>0.0204</b>	<b>0.0243</b>	<b>0.0377</b>	<b>0.0462</b>
			TI-DeepONet AB [Ours]	0.0264	0.0310	0.0473	0.0579
			Full Rollout	0.0433	0.0965	0.2413	0.3281
			Autoregressive	0.5898	0.8742	1.4682	1.7154
KdV (1D)	2.5	0.05	TI(L)-DeepONet [Ours]	0.0884	0.1133	<b>0.1295</b>	0.2010
			TI-DeepONet AB [Ours]	<b>0.0861</b>	<b>0.1114</b>	0.1330	<b>0.1941</b>
			Full Rollout	0.7769	0.7163	0.7197	0.7951
			Autoregressive	0.8127	0.8985	0.9691	1.0626
Burgers' (2D)	0.33	0.01	TI(L)-DeepONet [Ours]	<b>0.1093</b>	<b>0.1202</b>	<b>0.1419</b>	<b>0.1531</b>
			TI-DeepONet AB [Ours]	0.1238	0.1361	0.1609	0.1736
			Full Rollout	0.1275	0.1907	0.3649	0.4733
			Autoregressive	0.4969	0.5801	0.7604	0.8617

\*  $t_{train}^* = t$ : Beginning time of extrapolation;  $\Delta t_e$ : Evaluation timestep;  $T^*$ : Final prediction time.

with periodic BCs and IC,  $u(x, 0) = s(x)$ . We generated 2,500 realizations of  $s(x)$  and the corresponding solutions, splitting them into 2,000 training and 500 test samples. To evaluate temporal extrapolation, models were trained on  $t \in [0, 0.5]$  and tested on the full interval  $t \in [0, 1]$ .

In the full rollout setting, DeepONet learns a mapping  $\mathcal{G}_\theta: s(x) \mapsto u(x, t)$  using a branch network (for the IC) and a trunk network (for spatiotemporal coordinates). A single forward pass predicts the entire solution field. In the autoregressive setting, the models - Autoregressive DeepONet, TI-DeepONet, and TI(L)-DeepONet - the branch network takes as input the state of the system at the current timestep, and the trunk network takes only the spatial discretization. Autoregressive DeepONet predicts the solution at the next time step, while TI-DeepONet and TI(L)-DeepONet predict the time derivative of the solution at the current timestep and integrate temporal dynamics using numerical solvers. TI-DeepONet employs a Heun-type AB2/AM3 predictor–corrector scheme, defined as:

$$\hat{u}^{n+1} = u^n + \Delta t \left[ \frac{3}{2} \mathcal{F}(t^n, u^n) - \frac{1}{2} \mathcal{F}(t^{n-1}, u^{n-1}) \right], \quad (\text{Predictor}) \quad (4)$$

$$u^{n+1} = u^n + \Delta t \left[ \frac{5}{12} \mathcal{F}(t^{n+1}, \hat{u}^{n+1}) + \frac{8}{12} \mathcal{F}(t^n, u^n) - \frac{1}{12} \mathcal{F}(t^{n-1}, u^{n-1}) \right] \quad (\text{Corrector}) \quad (5)$$

Figure 4 illustrates the performance of all models for a representative test sample. All models perform well in the training interval; however, the autoregressive DeepONet accumulates error early and diverges during extrapolation. The quantitative trends presented in Table 1 underscore the qualitative observations from Figure 4 as well as Figure 3(a) and (b). The autoregressive DeepONet deteriorates rapidly during extrapolation due to cumulative errors without stabilization mechanisms. While full rollout DeepONet performs better due to its non-recursive architecture, it fails to maintain accuracy beyond the training interval since it does not leverage the Markovian structure of time-dependent PDEs.

In contrast, the proposed TI-DeepONet variants, which embed numerical integration schemes into the learning framework, demonstrate superior extrapolation accuracy (see Figure 3(b)). TI-DeepONet with AB2/AM3 integration effectively stabilizes long-horizon predictions. TI(L)-DeepONet further improves on this by learning adaptive RK4 slope coefficients conditioned on the current state, enabling it to modulate time-stepping dynamically in response to the local solution behavior. This is particularly beneficial in stiff or nonlinear regimes, as reflected in the consistently lowest errors observed across all time steps. Figure A1 in SI presents iteration-wise learning of the RK4 slope coefficients, comparing it against the reference. An important point to note here is that the obtained

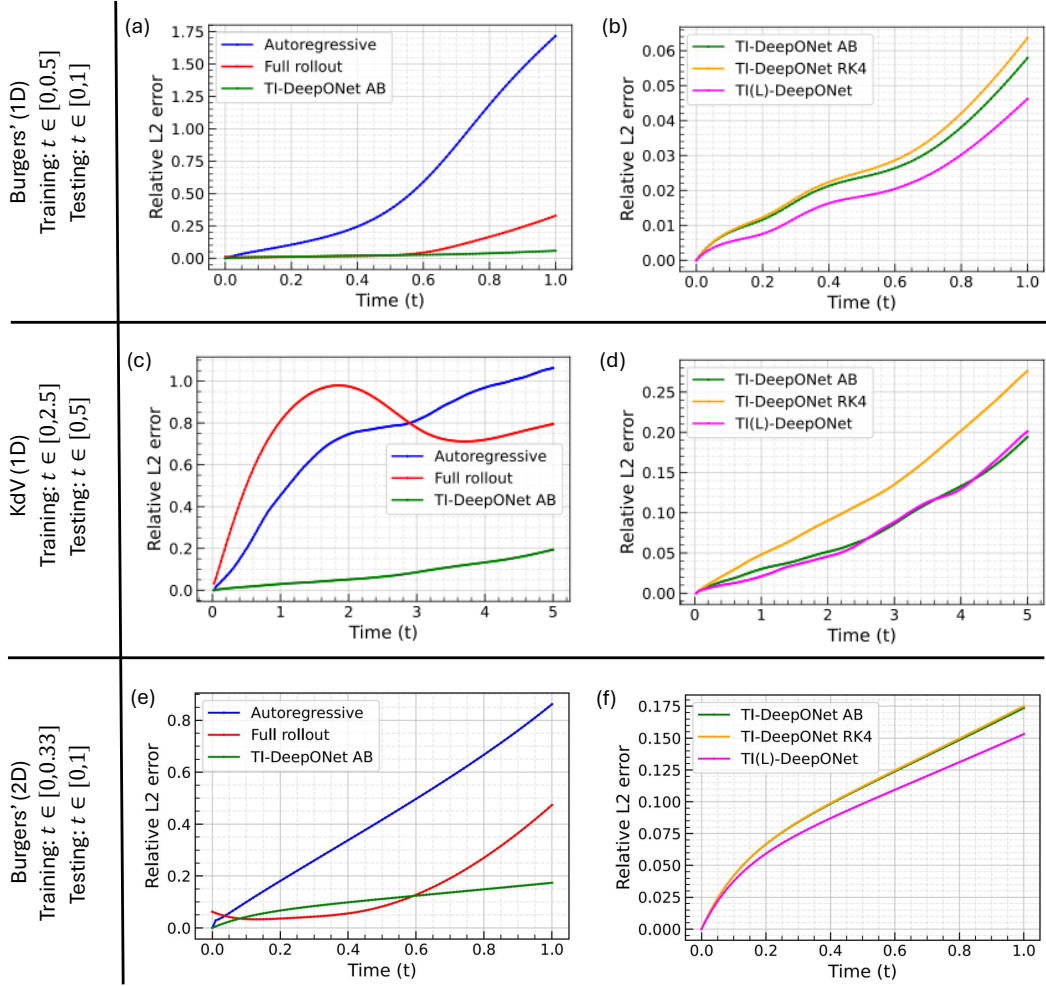


Figure 3: Temporal evolution of the relative  $L_2$  error for different frameworks in all applications. Left: Comparison of baseline models with TI-DeepONet AB, which uses RK4 during training and AB2/AM3 during inference. Right: Comparison among TI-based variants. TI-DeepONet RK4 employs RK4 integration in both training and inference, while TI(L)-DeepONet adapts RK4 coefficients via a learnable scheme conditioned on the input state.

optimized coefficients are compensating for the approximation error of the TI-DeepONet; hence, they may not necessarily adhere to the values obtained using the Taylor series expansion.

### 3.2 One-dimensional Korteweg-de Vries (KdV) Equation

The one-dimensional KdV equation models nonlinear dispersive waves and arises in contexts such as shallow water dynamics, plasma physics, and lattice acoustics. It introduces third-order dispersion into the Burgers-like formulation:

$$\frac{\partial u}{\partial t} - \eta u \frac{\partial u}{\partial x} + \gamma \frac{\partial^3 u}{\partial x^3} = 0, \quad (6)$$

where,  $u$  is the amplitude of the wave,  $\gamma$  and  $\eta$  are some real-valued scalar parameters,  $x$  and  $t$  are the spatial and temporal dimensions, respectively. We generated 1,000 initial conditions to simulate time evolution, splitting them into 800 for training and 200 for testing.

Figure 5 presents predictions from different frameworks on a representative sample. Both the full rollout and autoregressive DeepONet models fail to capture the dispersive, periodic dynamics of the solution. The full rollout approach, which treats time steps independently, lacks temporal continuity, while the autoregressive model suffers from compounding errors during recursive inference. In

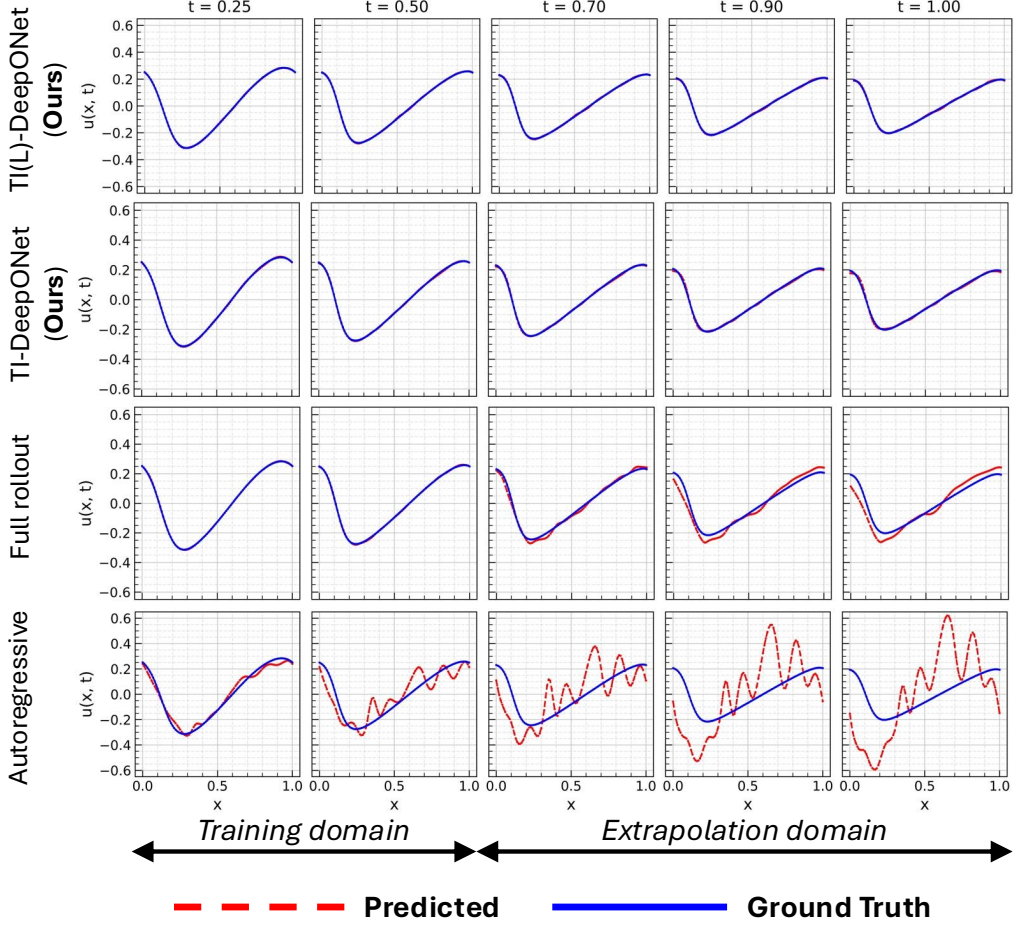


Figure 4: 1D Burgers’ equation: Performance of all frameworks in the training ( $t \in [0, 0.5]$ ) and extrapolation ( $t \in [0.5, 1]$ ) regimes for a representative sample.

contrast, TI-DeepONet and TI(L)-DeepONet closely match the ground truth, even in the extrapolation regime. The adaptive RK4 scheme in TI(L)-DeepONet yields similar accuracy as TI-DeepONet. Figures 3(c) and (d) show the relative  $L_2$  error over time. The autoregressive DeepONet exhibits rapid error growth beyond  $t = 2.5$ , while the full rollout model shows non-monotonic behavior due to its limited ability to model coherent temporal evolution. In comparison, the TI-based models maintain low and stable errors across the prediction window. At  $t = 5$ , TI(L)-DeepONet and TI-DeepONet achieve final errors of approximately 20% and 19.4%, respectively, 4-5 $\times$  lower than baseline methods. The performance difference between TI-DeepONet with AB2/AM3 and TI(L)-DeepONet is marginal, indicating that both are reliable choices for long-term modeling of PDEs similar to the KdV equation.

### 3.3 Two-dimensional Burgers’ Equation

To assess performance on high-dimensional spatiotemporal dynamics, we consider the 2D Burgers’ equation, defined as:

$$\frac{\partial u}{\partial t} + u \frac{\partial u}{\partial x} + u \frac{\partial u}{\partial y} = \nu \left( \frac{\partial^2 u}{\partial x^2} + \frac{\partial^2 u}{\partial y^2} \right), \quad \forall (x, y, t) \in [0, 1]^2 \times [0, 1], \quad (7)$$

where  $u(x, y, t)$  is a scalar field and  $\nu = 0.01$  is the kinematic viscosity. The IC,  $u(x, y, 0) = s(x, y)$  is sampled from 2D Gaussian random fields, and periodic Dirichlet and Neumann BCs are applied in both  $x$  and  $y$  directions.

Figure 6 presents the spatial error plots in the training and the extrapolation regimes, demonstrating the time integrator models to be significantly more accurate than the baseline models. The solution plot for the same sample is presented in Figure A2. Figure 3 (e) and (f) compares the relative  $L_2$  error

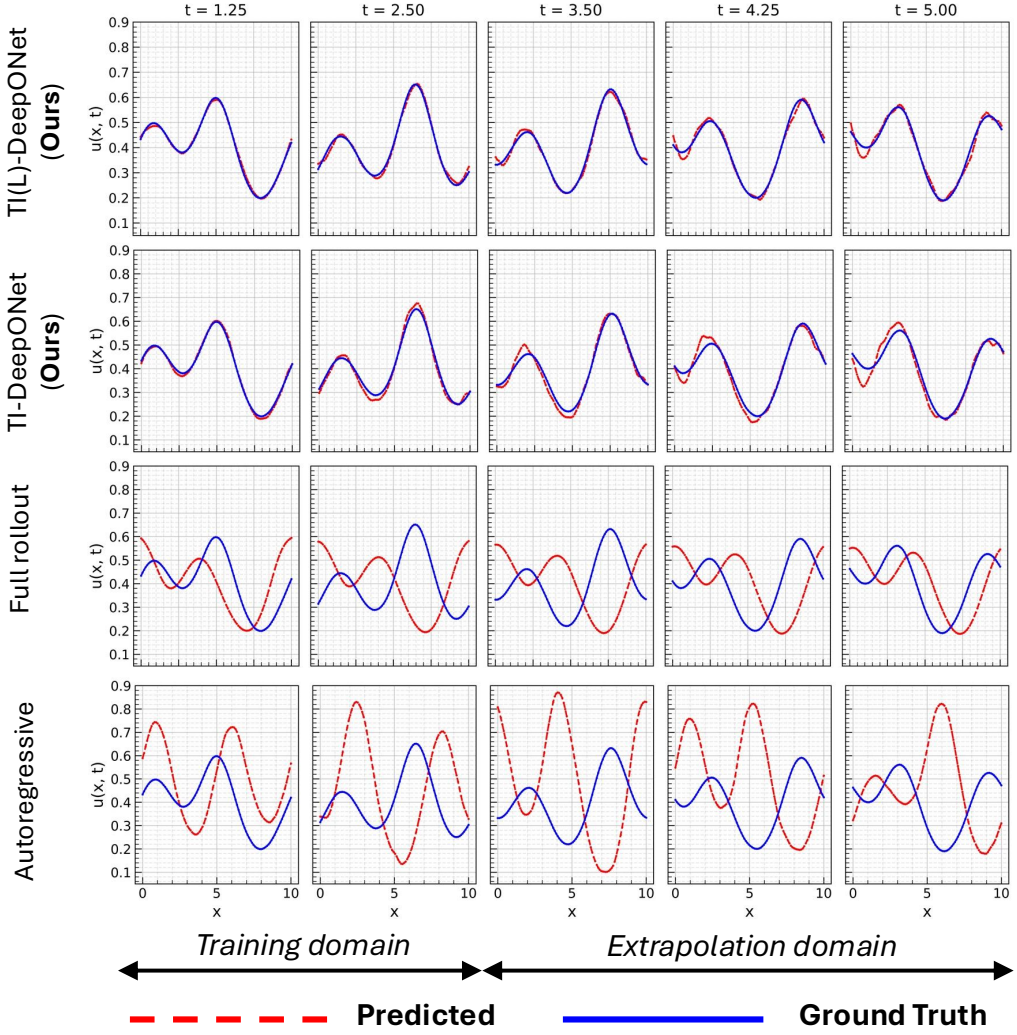


Figure 5: 1D KdV equation: Performance of all the frameworks in the training ( $t \in [0, 2.5]$ ) and the extrapolation regime ( $t \in [2.5, 5]$ ) for a representative sample.

trends over the entire temporal domain. The autoregressive DeepONet rapidly accumulates error, exceeding 85% by the final time step. The full rollout DeepONet initially performs better, but its fixed-basis representation limits its temporal generalization, and errors surpass TI-DeepONet beyond  $t = 0.5$ . Similar to the previous examples, TI(L)-DeepONet maintains slow error growth, with final errors around 15%, outperforming all baselines and the TI-DeepONet model in the long-term prediction regime. These results demonstrate the robustness of the time-integrator frameworks in modeling complex spatiotemporal dynamics.

## 4 Conclusions

Accurate long-term extrapolation of dynamical systems remains a fundamental challenge for neural operators, particularly due to error accumulation in autoregressive predictions. To address this, we introduce TI-DeepONet and its adaptive variant TI(L)-DeepONet, which integrates classical numerical time integration with an operator learning framework (DeepONet). By reformulating the learning objective to approximate instantaneous time derivatives-subsequently integrated via high-order numerical schemes, our frameworks preserve the causal structure of dynamical systems while enhancing stability and accuracy in long-term forecasting. Furthermore, the operator learning paradigm enables continuous spatiotemporal solutions for parametrized initial conditions, thereby enabling the construction of an efficient and reliable emulator for complex systems. Extensive

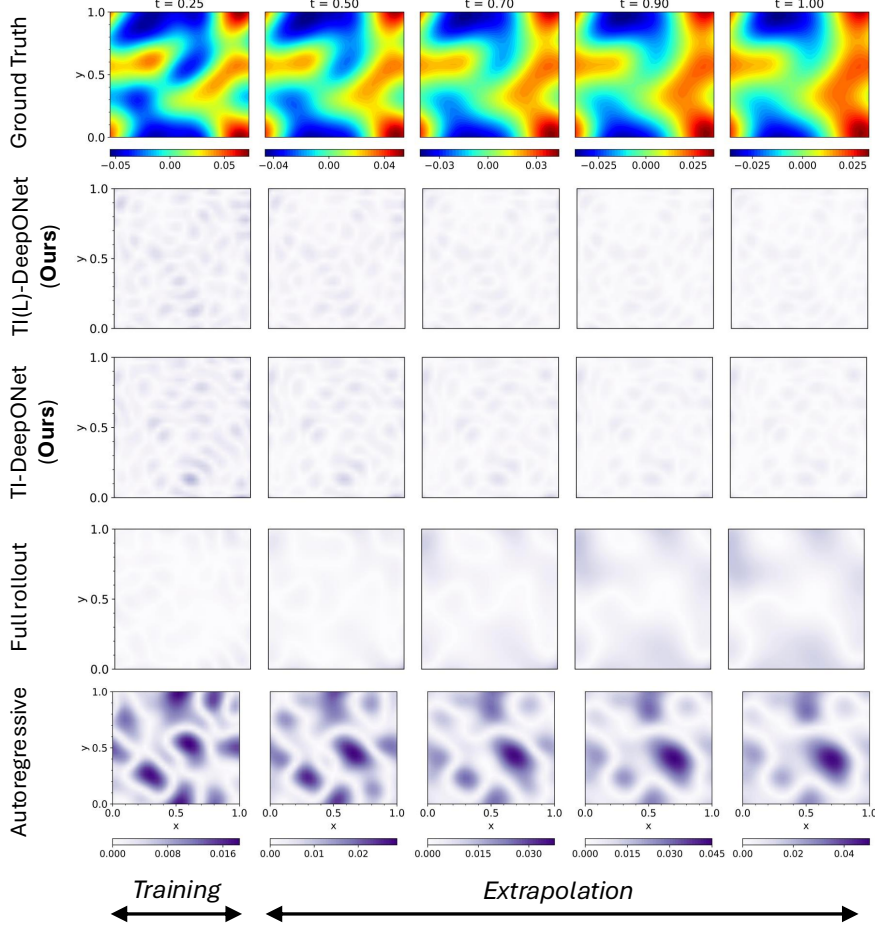


Figure 6: 2D Burgers’ equation: Spatial error distribution across training ( $t \in [0, 0.33]$ ) and extrapolation ( $t \in [0.33, 1]$ ) regimes for all frameworks, illustrated with a representative sample.

evaluations across three canonical PDEs (1D/2D Burgers’ and 1D KdV equations) demonstrate the superiority of our approach. TI-DeepONet reduces relative  $L_2$  extrapolation errors by 81% compared to autoregressive DeepONet and 70% compared to full-rollout methods, while maintaining stable predictions for temporal domains extending up to twice the training interval. The learnable coefficients in TI(L)-DeepONet further refine accuracy by adaptively weighting intermediate integration slopes, enabling solution-specific adjustments that outperform static numerical schemes in all our examples. By embedding temporal causality into the learning process and decoupling training-time integrators (e.g., Runge-Kutta) from inference-time integrators (e.g., Runge-Kutta or Adams-Basforth), our methodology bridges neural operator flexibility with the robustness of numerical analysis. Among the proposed variants, TI(L)-DeepONet achieves the highest accuracy, albeit with a higher per-iteration computational cost due to its learnable integration coefficients (see SI Section A). However, this increase is offset by its significantly faster convergence to lower training loss, resulting in no net increase in total compute time. This hybrid paradigm offers a reliable pathway for modeling high-dimensional, time-dependent systems, where stability and generalizability are critical.

## 5 Limitations and Future Work

While our proposed frameworks demonstrate superior extrapolation accuracy compared to existing neural operator training strategies, they incur higher computational costs during both training and inference, as detailed in the SI Section A. Although these offline training costs can be justified by the consistent reliability of predictions across a wide range of parametric initial conditions, improving computational efficiency remains a key priority. To this end, we plan to leverage multi-GPU training and investigate methods for more efficient forward and backward propagation through the ODE

solver. Additionally, we aim to extend the framework’s scalability to 3D and multiphysics systems and to incorporate adaptive time-stepping strategies for handling stiff dynamical systems.

## Acknowledgments

The authors’ research efforts were partly supported by the National Science Foundation (NSF) under Grant No. 2438193 and 2436738. The authors would like to acknowledge computing support provided by the Advanced Research Computing at Hopkins (ARCH) core facility at Johns Hopkins University and the Rockfish cluster. ARCH core facility (`rockfish.jhu.edu`) is supported by the NSF grant number OAC1920103. Any opinions, findings, conclusions, or recommendations expressed in this material are those of the author(s) and do not necessarily reflect the views of the funding organizations.

## References

- [1] Lu Lu, Pengzhan Jin, Guofei Pang, Zhongqiang Zhang, and George Em Karniadakis. Learning nonlinear operators via DeepONet based on the universal approximation theorem of operators. *Nature machine intelligence*, 3(3):218–229, 2021.
- [2] Zongyi Li, Nikola Borislavov Kovachki, Kamyar Azizzadenesheli, Kaushik Bhattacharya, Andrew Stuart, Anima Anandkumar, et al. Fourier Neural Operator for Parametric Partial Differential Equations. In *International Conference on Learning Representations*.
- [3] Guang Lin, Christian Moya, and Zecheng Zhang. Learning the dynamical response of nonlinear non-autonomous dynamical systems with deep operator neural networks. *Engineering Applications of Artificial Intelligence*, 125:106689, 2023.
- [4] Sifan Wang and Paris Perdikaris. Long-time integration of parametric evolution equations with physics-informed DeepONets. *Journal of Computational Physics*, 475:111855, 2023.
- [5] Wuzhe Xu, Yulong Lu, and Li Wang. Transfer Learning Enhanced DeepONet for Long-Time Prediction of Evolution Equations. In *Proceedings of the AAAI Conference on Artificial Intelligence*, volume 37, pages 10629–10636, 2023.
- [6] W Diab and M Al Kobaisi. Temporal extrapolation and reliable generalization via 2u-nets deep operator network (2u-deeponet) for time-dependent pdes. In *ECMOR 2024*, volume 2024, pages 1–16. European Association of Geoscientists & Engineers, 2024.
- [7] Lizuo Liu and Wei Cai. Deeppropnet—a recursive deep propagator neural network for learning evolution pde operators. *arXiv preprint arXiv:2202.13429*, 2022.
- [8] Waleed Diab and Mohammed Al-Kobaisi. Temporal Neural Operator for Modeling Time-Dependent Physical Phenomena. *arXiv preprint arXiv:2504.20249*, 2025.
- [9] Katarzyna Michałowska, Somdatta Goswami, George Em Karniadakis, and Signe Riemer-Sørensen. Neural operator learning for long-time integration in dynamical systems with recurrent neural networks. In *2024 International Joint Conference on Neural Networks (IJCNN)*, pages 1–8. IEEE, 2024.
- [10] Ricardo Buitrago, Tanya Marwah, Albert Gu, and Andrej Risteski. On the Benefits of Memory for Modeling Time-Dependent PDEs. In *The Thirteenth International Conference on Learning Representations*.
- [11] Junyan He, Shashank Kushwaha, Jaewan Park, Seid Koric, Diab Abueidda, and Iwona Jasiuk. Sequential deep operator networks (S-DeepONet) for predicting full-field solutions under time-dependent loads. *Engineering Applications of Artificial Intelligence*, 127:107258, 2024.
- [12] Zheyuan Hu, Qianying Cao, Kenji Kawaguchi, and George Em Karniadakis. DeepOMamba: State-Space Model for Spatio-Temporal PDE Neural Operator Learning. Available at *SSRN 5149007*.
- [13] Ricky TQ Chen, Yulia Rubanova, Jesse Bettencourt, and David K Duvenaud. Neural ordinary differential equations. *Advances in neural information processing systems*, 31, 2018.
- [14] Tianping Chen and Hong Chen. Universal approximation to nonlinear operators by neural networks with arbitrary activation functions and its application to dynamical systems. *IEEE transactions on neural networks*, 6(4):911–917, 1995.

- [15] Samuel Lanthaler, Siddhartha Mishra, and George E Karniadakis. Error estimates for DeepONets: a deep learning framework in infinite dimensions. *Transactions of Mathematics and Its Applications*, 6(1):tnac001, 2022.

## A Limitations: Computational costs

The improved extrapolation accuracy offered by the proposed TI-DeepONet and TI(L)-DeepONet approaches comes at the cost of increased training and inference times. This additional computational overhead stems from the repeated forward and backward passes through the time integrator. However, the convergence of TI-based networks is significantly faster, indicating more efficient optimization of network parameters compared to baseline methods. Table A1 presents a detailed comparison of the training and inference costs for each method across all benchmark problems. Moreover, incorporating adaptive, learnable slope coefficients facilitates convergence to the true solution even faster due to the solution-specific local adaptivity within the time integrator. Training and inference for the 1D Burgers' and 1D KdV cases were conducted on a single NVIDIA A100 GPU equipped with 40GB memory (Intel Xeon Gold Cascade Lake). The 2D Burgers' case was performed on a NVIDIA A100 GPU with 80GB memory (Intel Xeon Gold Icy Lake).

Table A1: Computational costs of training and inference for all examples across different frameworks.

Problem	Method	Batch size	Training time (iter/sec)	$N_{test}$	Inference time (sec)
Burgers' (1D)	TI(L)-DeepONet (Ours)	256	163.62	2500	5.48
	TI-DeepONet AB (Ours)		195.43		5.86
	Full rollout		283.94		0.38
	Autoregressive		296.09		6.61
KdV (1D)	TI(L)-DeepONet (Ours)	256	179.82	1000	4.61
	TI-DeepONet AB (Ours)		208.59		4.47
	Full rollout		234.98		1.22
	Autoregressive		298.44		5.98
Burgers' (2D)	TI(L)-DeepONet (Ours)	128	32.83	1000	7.29
	TI-DeepONet AB (Ours)		37.42		6.98
	Full rollout		218.68		1.16
	Autoregressive		115.72		1.95

**Training cost analysis:** During training, the computational complexity varies across methods. The branch network requires  $\mathcal{O}(bs)$  forward passes per iteration, where  $bs$  represents the batch size. The trunk network evaluation complexity depends on the strategy employed:

- Full rollout:  $\mathcal{O}(n_s \times n_t)$  forward passes, where  $n_s$  is the number of spatial points and  $n_t$  is the number of temporal locations.
- Autoregressive methods (autoregressive DeepONet, TI-DeepONet, and TI(L)-DeepONet):  $\mathcal{O}(n_s)$  forward passes because of the absence of temporal dimension.

For TI(L)-DeepONet, an additional  $\mathcal{O}(bs)$  forward passes are required per iteration to evaluate the auxiliary deep neural network that learns the intermediate RK4 slopes. As a result, TI(L)-DeepONet incurs the highest per-iteration cost, leading to the lowest iteration speed observed in Table A1. Although TI-DeepONet and autoregressive DeepONet evaluate a similar number of forward passes, TI-DeepONet additionally invokes the time integrator, introducing extra forward computations. Consequently, it is more expensive to train than autoregressive DeepONet but still cheaper than TI(L)-DeepONet. The cost of the full rollout method scales directly with the spatiotemporal resolution. While it avoids recursion, the simultaneous prediction over all space-time points makes it more expensive than autoregressive methods, which predicts for only spatial points at each step. The trends observed in Table A1 align with this analysis. Note that in the 2D Burgers' case, the relatively higher training cost incurred by the autoregressive DeepONet is due to the use of additional hidden layers in the trunk network.

**Inference cost analysis:** During inference, full rollout is the fastest method, requiring  $\mathcal{O}(N_{test}) + \mathcal{O}(n_s \times n_t)$  forward passes for total evaluation, where  $N_{test}$  is the number of test samples. In contrast, the autoregressive, TI-DeepONet, and TI(L)-DeepONet methods perform recursive time predictions, resulting in longer inference times. For evaluating  $N_{test}$  samples, the autoregressive

networks simulate  $n_t \times \mathcal{O}(N_{\text{test}}) + n_t \times \mathcal{O}(n_s)$  forward passes. During inference, the additional network in the TI(L)-DeepONet is not evaluated as the optimized parameters are already obtained, resulting in no additional cost.

## B Statistical Variability

To evaluate the performance of the model, we compute the relative  $L_2$  error of the extrapolation predictions, and report the mean and standard deviation of this metric based on five independent training trials in Table A2.

Table A2: Relative  $L_2$  errors reported based on five independent training trials for all frameworks in the extrapolation regime.

Problem	Method	Relative $L_2$ error			
		$t+10\Delta t_e$	$t+20\Delta t_e$	$t+40\Delta t_e$	$T^*$
Burgers' (1D)	TI(L)-DeepONet	<b><math>0.019 \pm 0.003</math></b>	<b><math>0.023 \pm 0.003</math></b>	<b><math>0.036 \pm 0.004</math></b>	<b><math>0.044 \pm 0.005</math></b>
	TI-DeepONet AB	$0.031 \pm 0.004$	$0.037 \pm 0.005$	$0.057 \pm 0.008$	$0.070 \pm 0.011$
	Full Rollout	$0.043 \pm 0.002$	$0.095 \pm 0.004$	$0.247 \pm 0.028$	$0.336 \pm 0.053$
	Autoregressive	$0.710 \pm 0.089$	$1.004 \pm 0.144$	$1.556 \pm 0.206$	$1.768 \pm 0.227$
KdV (1D)	TI(L)-DeepONet	<b><math>0.054 \pm 0.019</math></b>	<b><math>0.065 \pm 0.027</math></b>	<b><math>0.075 \pm 0.031</math></b>	<b><math>0.111 \pm 0.051</math></b>
	TI-DeepONet AB	$0.086 \pm 0.026$	$0.108 \pm 0.034$	$0.129 \pm 0.043$	$0.183 \pm 0.063$
	Full Rollout	$0.776 \pm 0.0004$	$0.716 \pm 0.0005$	$0.719 \pm 0.0005$	$0.795 \pm 0.0007$
	Autoregressive	$0.823 \pm 0.073$	$0.886 \pm 0.064$	$0.922 \pm 0.069$	$0.968 \pm 0.083$
Burgers' (2D)	TI(L)-DeepONet	<b><math>0.111 \pm 0.002</math></b>	<b><math>0.121 \pm 0.003</math></b>	<b><math>0.143 \pm 0.004</math></b>	<b><math>0.155 \pm 0.004</math></b>
	TI-DeepONet AB	$0.121 \pm 0.002$	$0.133 \pm 0.002$	$0.157 \pm 0.003$	$0.169 \pm 0.003$
	Full Rollout	$0.131 \pm 0.007$	$0.194 \pm 0.014$	$0.357 \pm 0.035$	$0.453 \pm 0.049$
	Autoregressive	$0.503 \pm 0.017$	$0.590 \pm 0.024$	$0.783 \pm 0.052$	$0.894 \pm 0.075$

Across five independent trial runs, TI(L)-DeepONet consistently achieves the lowest extrapolation error across all benchmark problems. In addition to superior accuracy, it also exhibits reduced variance in error estimates, indicating enhanced robustness and reliability. It is noteworthy that in a single run of the 1D KdV problem, TI(L)-DeepONet and TI-DeepONet-AB exhibit comparable performance under a single random initialization (see Table 1). However, the superiority of TI(L)-DeepONet becomes clear when averaged over multiple seeds. As expected, both the full rollout and autoregressive DeepONet models suffer from substantially higher errors, particularly outside the training-time domain. Overall, the TI-based frameworks not only enhance extrapolation accuracy but also offer greater robustness across random initializations, underscoring their effectiveness for modeling time-dependent PDEs.

## C Additional details

### C.1 One-dimensional Burgers' Equation

**Data generation:** The initial condition  $s(x)$  is sampled from a Gaussian random field with spectral density  $S(k) = \sigma^2(\tau^2 + (2\pi k)^2)^{-\gamma}$ , where  $\sigma = 25$ ,  $\tau = 5$ , and  $\gamma = 4$ . This ensures  $s(x)$  is periodic on  $x \in [0, 1]$ . The corresponding kernel is expressed via inverse Fourier transform as  $K(\mathbf{x}, \mathbf{x}') = \int_{-\infty}^{\infty} S(k) e^{2\pi i k(\mathbf{x} - \mathbf{x}')} dk$ . We discretize the spatiotemporal domain using 101 grid points along each dimension.

**Data preparation:** The training and testing datasets are constructed differently depending on the learning strategy employed. In the full rollout setting, where the goal is to train a DeepONet to learn a solution operator  $\mathcal{G}_{\theta}$  that maps an initial condition  $s(x)$  to the full spatiotemporal solution  $u(x, t)$ , we consider a set of initial conditions, spatiotemporal query locations, and the corresponding

solution field. The data is partitioned into training and testing sets using a train-test split ratio of 0.8. Specifically, we use  $N_{\text{train}} = 2000$  and  $N_{\text{test}} = 500$  samples. Additionally, recall that we are interested in assessing the performance of the various DeepONet frameworks in learning the full spatiotemporal field over the entire temporal domain, when it has access to the solution at limited timesteps. In this regard, we consider only half of the temporal domain, i.e.,  $t_{\text{train}} \in [0, 0.5]$  during training. Consequently, the grid for the trunk network is formed by taking a meshgrid over spatiotemporal coordinates,  $(x, t)$ , where  $x \in [0, 1]$  and  $t = t_{\text{train}} \in [0, 0.5]$  during training and  $t \in [0, 1]$  during testing.

For training the autoregressive DeepONet, TI-DeepONet and TI(L)-DeepONet architectures, we adopt a different strategy for preparing the training and testing datasets. In the case of autoregressive methods, the future states of the system are recursively predicted using the model’s own previous outputs as inputs at each timestep. This approach inherently leads to error accumulation, as prediction errors at one timestep are propagated and potentially amplified in the future timesteps. Understanding and mitigating this issue is a key motivation behind the TI-DeepONet architecture. In this regard, the training dataset is created as follows. The input to the branch network is formed by stacking the solution states from  $t = 0$  to  $t = 0.5$ , i.e., the dataset  $[u^0(x), u^1(x), \dots, u^{50}(x)]$ . Similarly, the output ground truth is formed by stacking the solution states from  $t = 0.01$  to  $t = 0.51$ , i.e., the dataset  $[u^1(x), u^2(x), \dots, u^{51}(x)]$ . The rationale behind arranging the dataset in such a way is that in this case, we aim to model the solution operator  $\mathcal{G}_{\theta}$  to learn the mapping:  $u^i(x) \rightarrow u^{i+1}(x)$ , where  $u^i(x)$  and  $u^{i+1}(x)$  are the solution states at the  $i^{\text{th}}$  and  $(i+1)^{\text{th}}$  timesteps, respectively. The trunk network processes only the spatial coordinates  $x \in [0, 1]$ .

**Training architecture:** Table A3 presents the network architecture details, including the number of layers and neurons per layer, activation functions, total epochs to convergence, and batch size. For the TI(L)-DeepONet architecture, we additionally employ an auxiliary feedforward network designed to predict the four RK4 slope coefficients. This network consists of two hidden layers with 32 neurons each, followed by an output layer with four neurons. The hidden layers use the `tanh` activation function, while a `softmax` activation is applied at the output layer to ensure the predicted coefficients sum to one. Training was performed using the Adam optimizer with an initial learning rate of  $10^{-3}$ , which was exponentially decayed by a factor of 0.95 every 5000 epochs. A similar learning rate scheduling strategy was employed for the auxiliary network predicting the adaptive RK4 slope coefficients. Both train and test losses were monitored at each epoch of training. The final model corresponds to the set of parameters that yielded the lowest test loss over the entire training process. Among all the tested architectures, TI(L)-DeepONet exhibited the fastest convergence, attributed to its capacity to adapt to the local dynamics of the solution. Later in this section, we examine the evolution of the learned RK4 slope coefficients across epochs and compare them to the reference coefficients:  $\frac{1}{6}, \frac{2}{6}, \frac{2}{6}, \frac{1}{6}$ .

Table A3: 1D Burgers’ equation: Neural network architecture and training settings across different methods.

Method	Branch Net	Trunk Net	Activation	Epochs	Batch Size
TI(L)-DeepONet	[101], [100]×6, [60]	[100]×6, [60]	Tanh	$1 \times 10^5$	256
TI-DeepONet	[101], [100]×6, [60]	[100]×6, [60]	Tanh	$1 \times 10^5$	256
Full rollout	[128]×6, [60]	[128]×6, [60]	Tanh	$2 \times 10^5$	256
Autoregressive	[101], [100]×6, [60]	[100]×6, [60]	Tanh	$1 \times 10^5$	256

**Learnable Weights:** As previously discussed, the learnable slope coefficients  $\alpha = [\alpha_1, \alpha_2, \alpha_3, \alpha_4]$  are predicted by the additional MLP, which takes the current solution state  $u^i$  as input, i.e.,  $\alpha = \text{MLP}_{\theta}(u^i)$ . Analyzing the evolution of these solution-specific coefficients over training epochs provides insight into how the network adapts the time integrator to local dynamics, in contrast to using a fixed set of RK4 coefficients. This comparison is illustrated in Fig. A1. The dashed blue line in each plot indicates the reference slope coefficients typically used in the RK4 method, derived from a Taylor series expansion. These coefficients result in a fourth-order accurate scheme and are generally expected to provide high accuracy for traditional time integrators. However, in the context of the operator learning framework, these coefficients also adapt to the approximation error of the

neural operator. Making these slope coefficients learnable allows the model to better compensate for such errors, thereby improving the overall accuracy of the framework.

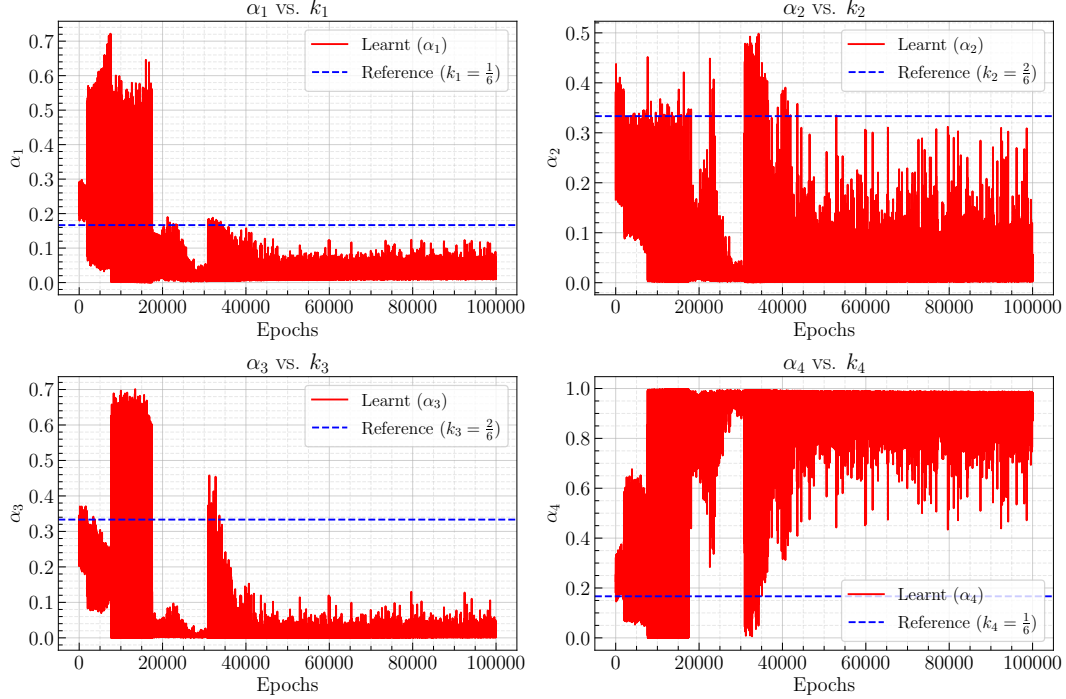


Figure A1: 1D Burgers' Equation: Epoch-wise change of the learnable RK4 slope coefficients  $\alpha = [\alpha_1, \alpha_2, \alpha_3, \alpha_4]$ .

## C.2 One-dimensional Korteweg-de Vries (KdV) Equation

**Data generation:** The initial condition,  $u(x, 0)$  is defined as a sum of two solitons, i.e.,  $u = u_1 + u_2$ . A soliton is a nonlinear, self-reinforcing, localized wave packet that is strongly stable. It is expressed as:

$$u_i(x, 0) = 2k_i^2 \operatorname{sech}^2 \left( k_i \left( \left( x + \frac{P}{2} - Pd_i \right) \%P - \frac{P}{2} \right) \right)^2 \quad (8)$$

where  $\operatorname{sech}$  is hyperbolic secant,  $P$  is the period in space,  $\%$  is the modulo operator,  $i = \{1, 2\}$ ,  $k \in [0.5, 1]$  and  $d \in [0, 1]$  are the coefficients that determine the height and location of the soliton peak, respectively. The dataset is curated by generating  $N = 1000$  distinct initial conditions and their temporal evolution is modeled using the midpoint method. The 1D spatial domain,  $\Omega = [0, 10]$ , is discretized into 100 uniformly spaced grid points, resulting in a spatial resolution of  $\Delta x = 0.1$ . For the temporal domain, we consider a uniform grid of 201 points spanning the time domain  $t \in [0, 5]$ , which yields a  $\Delta t = 0.025$ .

**Data preparation:** To assess the extrapolation accuracy of the different methods, we train only on the first half of the temporal domain, i.e.,  $t_{\text{train}} \in [0, 2.5]$ , and evaluate the predictive performance over the entire domain ( $t \in [0, 5]$ ). To reiterate, in the full rollout setting, the inputs to the trunk network are constructed from a meshgrid of  $(x, t_{\text{train}})$ , whereas in the autoregressive setting, only the spatial coordinates ( $x$ ) are used as trunk inputs. Moreover, while the initial condition samples serve as the input to the branch network in the DeepONet full rollout model, the input to the branch network in the autoregressive and TI-based DeepONet frameworks consists of the stacked solution states from  $t = 0$  to  $t = 2.5$ , i.e.,  $[u^0(x), u^1(x), \dots, u^{100}(x)]$ . The train-test split is kept at 0.8.

**Training architecture:** Table A4 presents the network architecture details, including the number of layers, neurons per layer, activation functions, total epochs to convergence, and batch size.

Similarly, for the TI(L)-DeepONet framework, we employ a secondary feedforward network to predict the four RK4 slope coefficients. This network consists of two hidden layers with 64 and 48 neurons, respectively, followed by an output layer with four neurons. The hidden layers use the  $\tanh$  activation function, while a  $\text{softmax}$  activation is applied at the output layer to ensure that the predicted coefficients sum to one. Training was performed using the Adam optimizer with an initial learning rate of  $10^{-3}$ , which was exponentially decayed by a factor of 0.95 every 5000 epochs. A similar learning rate schedule was also used for training the auxiliary network tasked with learning the RK4 slope coefficients.

Table A4: 1D KdV equation: Neural network architecture and training settings across different methods.

Method	Branch Net	Trunk Net	Activation	Epochs	Batch Size
TI(L)-DeepONet	$[128] \times 6, [80]$	$[128] \times 6, [80]$	Tanh	$1.5 \times 10^5$	256
TI-DeepONet	$[128] \times 6, [80]$	$[128] \times 6, [80]$	Tanh	$1 \times 10^5$	256
Full rollout	$[150, 250, 450, 380, 320, 300, 80]$	$[200, 220, 240, 250, 260, 280, 300, 80]$	Swish	$1 \times 10^5$	256
Autoregressive	$[128] \times 6, [80]$	$[128] \times 6, [80]$	Tanh	$1 \times 10^5$	256

### C.3 Two-dimensional Burgers' Equation

**Data generation** In the 2D Burgers' transport dynamics problem, we consider periodic boundary conditions, where the solution  $u(t, x, y)$  is a scalar field, and the initial condition  $u_0(x, y)$  is sampled from a periodic Matérn-type GRF with length scale  $l = 0.125$  and standard deviation  $\sigma = 0.15$ .

**Data preparation** A total of  $N = 1000$  initial condition functions were generated. Each initial condition was discretized on a  $32 \times 32$  spatial grid, and the corresponding solution field was evolved over 101 uniformly spaced time steps, resulting in a spatiotemporal output field of size  $101 \times 32 \times 32$  for each of the 1000 initial condition realizations. The training and testing dataset were prepared using the same strategy as in the previous two cases.

In the full rollout setting, our aim is to learn a solution operator,  $\mathcal{G}_\theta$ , that performs the mapping:  $u_0(x, y) \rightarrow u(t, x, y)$ . Using a train-test split of 0.8, 800 realizations of initial conditions and their corresponding ground truth solutions were used for training, with 200 samples of initial conditions and ground truth solution fields kept aside for testing. The trunk network takes as input a triplet of spatiotemporal coordinates,  $(t, x, y)$ ; in a similar spirit to the previous cases, we only provide the first 33 out of 101 time steps during training. Thus, the input meshgrid for the trunk network is constructed using one-third of the temporal domain, i.e.,  $(t, x, y)$ , where  $t = t_{\text{train}} \in [0, 0.33]$ . For the autoregressive and TI-based frameworks, the input to the branch network consists of stacked solution states from  $t = 0$  to  $t = 0.33$ , i.e., the dataset  $[u^0(x, y), u^1(x, y), \dots, u^{33}(x, y)]$ . The trunk network in this case takes only the spatial coordinates  $(x, y)$  as input.

**Training architecture** Table A5 presents the network architecture details, including the number of layers and neurons per layer, activation functions, total epochs to convergence, and batch size. In this case, for the TI(L)-DeepONet architecture, we employ a similar combination of 2D convolutional blocks and MLP layers as used in the branch network to learn the RK4 slope coefficients. The convolutional blocks utilize the same combination of Conv2D and pooling layers as the branch, with the only difference being that the Conv2D layers have a reduced number of filters (32 instead of 64). This is followed by a flattening layer, after which the intermediate representation is passed through two fully connected hidden layers, each containing 32 neurons, and finally to an output layer with 4 neurons that predicts the RK4 slope coefficients.

The Conv2D layers use a ReLU activation function, the fully connected hidden layers use  $\tanh$ , and the output layer applies a  $\text{softmax}$  activation to ensure that the predicted slope coefficients sum to one. Training was performed using the Adam optimizer with an initial learning rate of  $10^{-3}$ , which was exponentially decayed by a factor of 0.95 every 5000 epochs. The auxiliary network responsible

for predicting the learnable RK4 slope coefficients was trained with a similar exponential decay schedule, but with a higher initial learning rate of  $5 \times 10^{-3}$ .

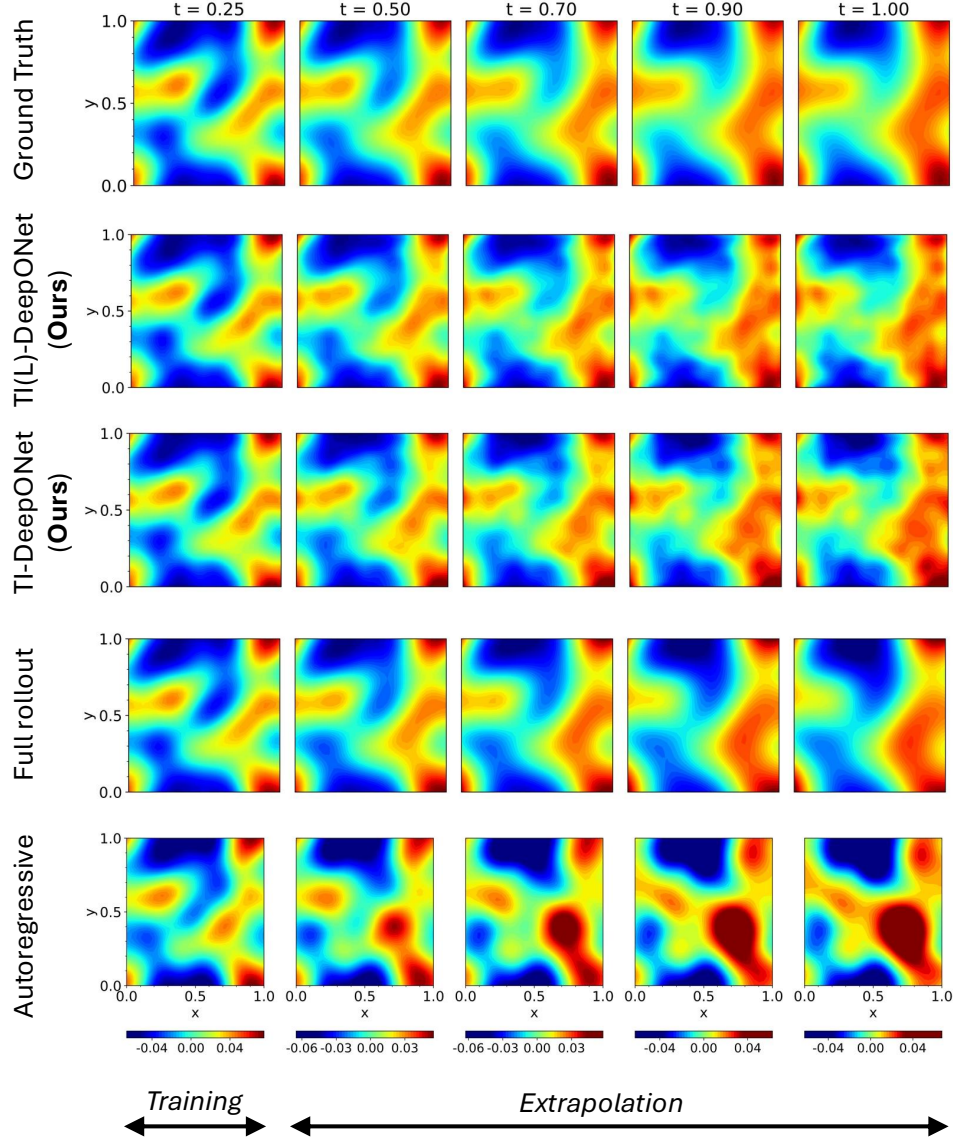


Figure A2: 2D Burgers' equation: Solution field for a representative sample, shown across both the training regime ( $t \in [0, 0.33]$ ) and the extrapolation regime ( $t \in [0.33, 1]$ ), for all frameworks. Corresponding error plots are presented in Figure 6.

Table A5: 2D Burgers' equation: Neural network architecture and training settings across different methods.

Method	Branch Net	Trunk Net	Activation	Epochs	Batch Size
TI(L)-DeepONet	Conv2D(features = 64, kernel size = (3,3), strides = 1), MaxPool(window shape=(2, 2), strides = (2, 2)), Conv2D(features = 64, kernel size = (2,2), strides = 1), AvgPool(window shape = (2,2), strides = (2,2)), MLP([256, 128, 100])	[128]×4, [100]	Conv2D: ReLU, MLP: Tanh	$1.5 \times 10^5$	64
TI-DeepONet	Conv2D(features = 64, kernel size = (3,3), strides = 1), MaxPool(window shape=(2, 2), strides = (2, 2)), Conv2D(features = 64, kernel size = (2,2), strides = 1), AvgPool(window shape = (2,2), strides = (2,2)), MLP([256, 128, 100])	[128]×4, [100]	Conv2D: ReLU, MLP: Tanh	$1.2 \times 10^5$	64
Full rollout	Conv2D(features = 64, kernel size = (3,3), strides = 1), MaxPool(window shape=(2, 2), strides = (2, 2)), Conv2D(features = 64, kernel size = (2,2), strides = 1), AvgPool(window shape = (2,2), strides = (2,2)), MLP([256, 128, 100])	[128]×3, [100]	Conv2D: ReLU, MLP: SiLU	$1 \times 10^5$	128
Autoregressive	Conv2D(features = 64, kernel size = (3,3), strides = 1), MaxPool(window shape=(2, 2), strides = (2, 2)), Conv2D(features = 64, kernel size = (2,2), strides = 1), AvgPool(window shape = (2,2), strides = (2,2)), MLP([256, 128, 100])	[128]×6, [100]	Conv2D: ReLU, MLP: SiLU	$1 \times 10^5$	64